Journal of Photonics for Energy

SPIEDigitalLibrary.org/jpe

Role of light scattering in the performance of fluorescent solar collectors

Nazila Soleimani
Sebastian Knabe
Gottfried H. Bauer
Tom Markvart
Otto L. Muskens

SPIE

Role of light scattering in the performance of fluorescent solar collectors

Nazila Soleimani,[a] Sebastian Knabe,[b] Gottfried H. Bauer,[b] Tom Markvart,[a] and Otto L. Muskens[c]

[a]University of Southampton, School of Engineering Sciences, Materials Research Group, Highfield, Southampton SO17 1BJ

[b]Carl von Ossietzky University of Oldenburg, Institute of Physics, D-26111 Oldenburg, Germany

[c]University of Southampton, SEPnet and Department of Physics and Astronomy, Highfield, Southampton SO17 1BJ

O.Muskens@soton.ac.uk

Abstract. A fluorescent solar collector (FSC) is a waveguide device that can concentrate both diffuse and direct sunlight on to a solar cell. The electrical output of the device depends strongly on the photon fluxes that are absorbed, emitted, and trapped inside the FSC plate. For this reason, it is important to study the photon transport losses inside the collector. One of the losses in FSC to be investigated is scattering, which increases the probability of the escape cone losses. We determine the scattering contributions in FSC by using angle dependence of light internally reflected in the FSC. The cause of scattering in spin-coated polymethylmethacrylate on top of the glass collector is identified as roughness from the top surface, rather than bulk losses. This loss can be suppressed to less than 2% using an index-matching planarization layer. [DOI: 10.1117/1.JPE.2.021801]

Keywords: fluorescent solar collector; solar energy; scattering; scattering measurements.

Paper 12014SS received Feb. 29, 2012; revised manuscript received Jul. 2, 2012; accepted for publication Jul. 17, 2012; published online Oct. 8, 2012.

1 Introduction

In a typical fluorescent solar collector (FSC), the luminescent light is trapped by total internal reflection (TIR) and guided to the edge of the plate, where it can be harvested by a solar cell. One objective of the collector design is to reduce the size of the solar cell with respect to the area that collects light. Unlike their geometric counterparts, fluorescent collectors can accept light from a wide angle of incidence and are thus able to make use of the diffuse light.[1] The photon flux at the edge of an idealized FSC is the product of the absorbed solar flux, the fraction of the trapped luminescence, and the geometric ratio of the area of the face directly exposed to sunlight A_f divided by the area A_e of the edge that is covered by the solar cell. The geometric gain G_{geom} of the FSC is then given by:

$$G_{\text{geom}} = \frac{A_f}{A_e}. \tag{1}$$

Weber and Lambe initially suggested the concept of luminescence trapping for solar concentrators, which they named the luminescent greenhouse collector.[2] In experimental FSC devices, the emitted photon flux is less than ideal due to several loss processes, including reabsorption and scattering.[1–9]

In this work, we investigate the effect of surface scattering in realistic FCS devices based on a dye-doped polymethylmethacrylate (PMMA) layer on top of a glass slide. To characterize the photon transport inside the collector, we monitor the angular distribution of a collimated light

0091-3286/2012/$25.00 © 2012 SPIE

beam, which enters the collector from the edge, after propagation and TIR. We find that the surface scattering process is described well by Fraunhofer diffraction at surface inhomogeneities several micrometers in size.

2 Theory

We calculate the effect of diffraction due to surface roughness on the FSC efficiency using the model developed by Weber and Lambe.[2] In their model, they included the guiding of light in the FSC at angles larger than the critical angle for total-internal-reflection, θ_c. Attenuation of reflected light by reabsorption is taken into account through an effective absorption coefficient α_e, while Fresnel reflection losses at the interface between the low-index FSC and the high-index solar cell is included through Fresnel's reflection coefficients for s- and p-polarized light.

In addition, we include here losses caused by angular spread of the reflected light due to surface roughness. The effect is included as a divergence of angles with a Gaussian profile of $1/e$ half-width $\Delta\theta$. Around the critical angle, this additional spread in angles results in part of the light being lost within the escape cone. The angular distribution of light remaining after one reflection from the rough surface can be approximated from the convolution of the unit step function with the Gaussian diffraction function, resulting in the error function $P(\theta) = \mathrm{erfc}[(\theta_c - \theta)/\Delta\theta]/2$. Under the condition that the scattering is only a small correction on the distribution function, the sequence of TIRs can be written as a multiplication of a number of error functions where the number is given by the amount of internal reflections from the rough surface. The total collection efficiency Q_C is defined as the total amount of light per unit length collected at the edge $y = L$ divided by the amount emitted per unit length. Inclusion of the surface scattering effect in the Weber and Lambe model results in an equation for Q_C given by

$$
\begin{aligned}
Q_C = (2\pi L)^{-1} \int_0^L \mathrm{d}y \int_0^{\pi/2} \mathrm{d}\phi \int_{\theta_c}^{\pi/2} \left\{ \frac{1}{2} \mathrm{erfc}[(\theta_c - \theta)/\Delta\theta] \right\}^{N_R(\theta,\phi)} \sin\theta \mathrm{d}\theta \\
\times \{ \exp[-\alpha_e (L - y)/\sin\theta \sin\phi] + \exp[-\alpha_e (L + y)/\sin\theta \sin\phi] \} \\
\times [2 - |r_s(\theta,\phi)|^2 - |r_p(\theta,\phi)|^2],
\end{aligned}
\tag{2}
$$

where θ and ϕ are the usual spherical polar angles defining the direction of emission, and the exponentials in Eq. (2) represent the Lambert-Beer law to estimate the absorption over the path length of a random ray within the collector over a distance $(L \pm y)$. The scattering losses depend on the total number of TIRs of light inside the collector. Here the number of TIRs from the rough surface is given by

$$
N_R(\theta,\phi) = \left\lfloor \frac{2L - y}{2T} \cot\theta \cot\phi \right\rfloor, \tag{3}
$$

where we have introduced the FSC thickness T. The brackets indicate the floor function that rounds N_R to the largest previous integer.

Results were calculated for the collection efficiency of the FSC for a representative collector with index $n_c = 1.5$ coupled into a semiconductor of index $n_s = 3.35$, i.e., the refractive index of GaAs used by Weber and Lambe.[2] We assumed a thickness given by $T = L/50$, which is typical for a medium-scale FSC device with a geometric gain of 50. Different values of T will change only the total amount of scattering loss, not the qualitative response. Figure 1(a) shows computed values obtained by numerical integration of Eq. (2). The curve in absence of surface scattering (closed circles) corresponds to the Weber and Lambe result.[2] Introduction of a surface roughness characterized by a $\Delta\theta = 1.5$ deg divergence results in a reduction of the efficiency by several percent (open circles). Also shown are the total (triangles) and relative (diamonds) scattering losses, where the latter is normalized to the collection efficiency for a smooth film ($\Delta\theta = 0$). The right-hand panel in Fig. 1 shows the absolute and relative scattering losses as a function of $\Delta\theta$ for a value of $\alpha_e L = 10^{-2}$, i.e., low reabsorption. Above $\Delta\theta = 1$ deg, the scattering loss increases roughly linearly with the diffraction width $\Delta\theta$. The loss percentage of 5% for $\Delta\theta = 2.5$ deg indicates the importance of surface roughness optimization in experimental FSC.

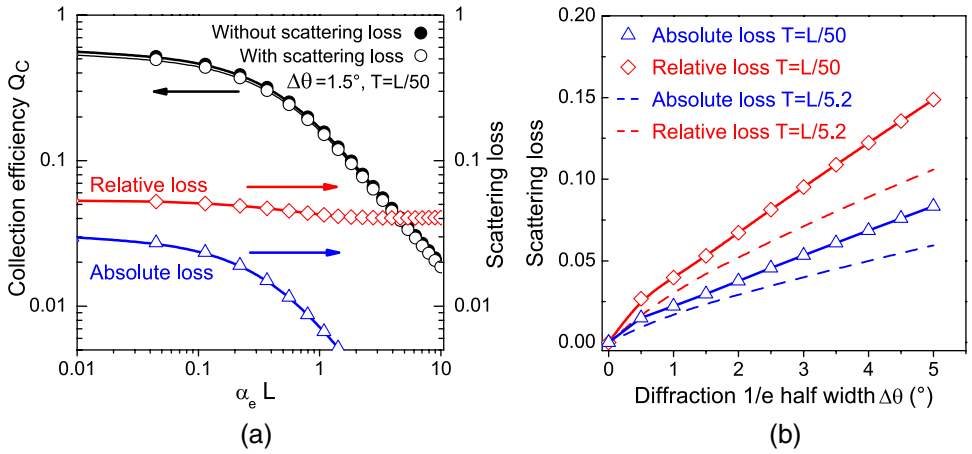

Fig. 1 (a) collection efficiency for the FSC as a function of $\alpha_e L$ calculated using the modified Weber and Lambe model Eq. (2), for a perfectly smooth surface ($\Delta\theta = 0$, closed dots) and a surface roughness characterized by $\Delta\theta = 1.5$ deg and $T = L/50$ (open dots). Blue triangles show absolute scattering loss, and red diamonds show relative scattering loss, normalized to the result for $\Delta\theta = 0$. (b) Blue triangles show absolute scattering long, and red diamonds show relative scattering loss, at $\alpha_e L = 10^{-2}$ as a function of the $1/e$ half width of the diffraction cone, for $T = L/50$ (symbols) and for $T = L/5.2$ (dashed lines).

For comparison, we have also shown the results for $T = L/5.2$, which corresponds to the small-scale experimental configuration in this work. As can be seen, the scattering loss does not scale linearly with the system size (i.e., the number of internal reflections), indicating that the majority of the loss is accumulated during the first few reflections. This can be understood from the fact that the angular range around the critical angle gets depleted of photons after the first few internal reflections, and therefore the effect saturates.

3 Method

3.1 *Sample*

The substrate used in this study was a BK7 glass slide with dimensions of $26 \times 26 \times 5$ mm^3. Before depositing the layers, the slides were thoroughly cleaned. A solution of 9% to 10% PMMA dissolved in Chlorobenzene (Micro Chem) was spin-coated (Laurell EDC-650-15TFM) at a speed of 4,000 rpm for 1 min. The thickness of the spin-coated layer was measured by using a profilometer (Talysurf-120 L, Taylor Hobson Ltd.) and was found to be 24.85 μm. The surface morphology of the PMMA layer was characterized using Atomic Force Microscopy (AFM). Figure 2 shows a representative AFM image, revealing that the layer shows a roughness of around 48 nm over a typical correlation length of several micrometers. This roughness may be associated with the relatively high thickness of PMMA required for fluorescent conversion in a realistic FSC, resulting in height variations during the spin-coating process. However, fluctuations may also be intrinsic to the polymer itself. Large-scale heterogeneities have been observed even in very pure PMMA, and its nature may be related to local alignment of polymer chains and strain produced during the drying process.[10]

3.2 *Scattering Setup*

For the characterization of light scattering, the samples were illuminated with a laser beam impinging from one side edge of the glass. The sample was placed at the center of a circular goniometer table illuminated with a laser. A silicon photodiode (SM05PD1A, Thorlabs) was mounted at the edge of the table as shown in Fig. 3. The distance between the sample and the detector was 27 cm. A pinhole with a diameter of 1 mm was placed in front of the silicon photodiode, which gives a solid angle for collection of 0.2 deg. A frequency of 185 Hz was

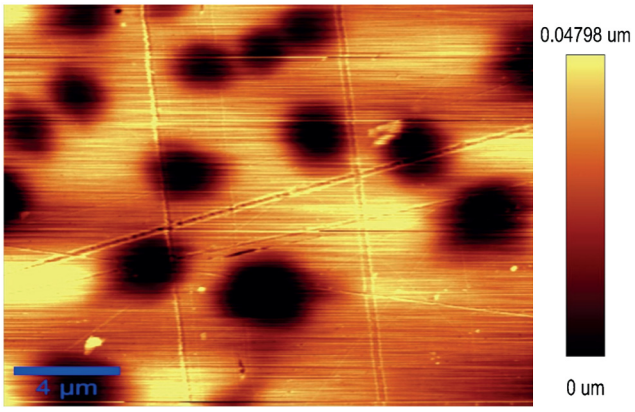

Fig. 2 Atomic Force Microscopy measurement of the PMMA layer.

applied via a chopper to the beam, and the current was detected by a photodiode connected via a lock-in amplifier (SR810). The lock-in amplifier was used to decrease the noise of the measurement by locking in to the chopper frequency, and the average of two current measurements, captured one second apart, was taken. The interface of this setup was programmed in Labview (8.6) software. A sample holder was fixed to the center of the goniometer table. The laser beam was aligned perpendicular to the surface of the sample, and the photodiode could be rotated around the table for measuring the scattered intensities at different angles. The scattered light intensity could be measured between 0 and 180 deg with a scattering angle increment of 0.5 deg.

3.3 *Scattering Measurement of FSC by Angular Dependence Method*

This section describes the method for measuring the scattering of PMMA spin-coated on top of the BK7 glass by illumination from one edge in different incident angles and detection from another edge. The geometry of the light illumination and reflection path through the glass is shown in Fig. 4. The distance of M (distance from detector inside of the glass) can be calculated by

$$\frac{\sin\theta_1}{\sin\theta_2} = \frac{n_2}{n_1} \quad \text{for } n_2 = 1.5 \quad \text{and} \quad n_1 = 1. \tag{4}$$

$$\tan\theta_2 = \frac{T}{2N}, \qquad N = 26 - M. \tag{5}$$

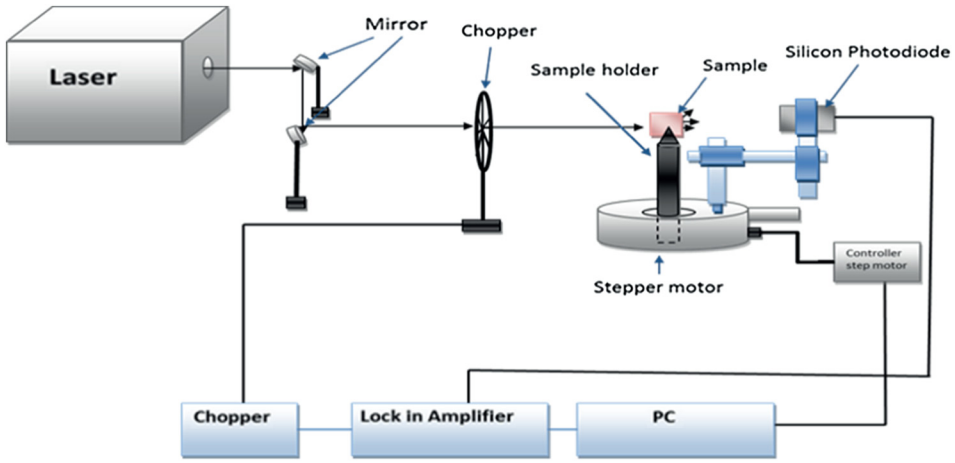

Fig. 3 Schematic of the experimental setup for the angle-dependent scattering measurements.

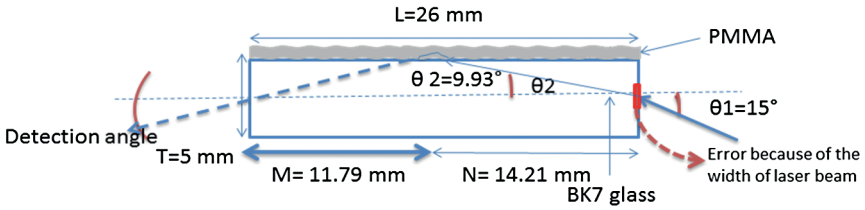

Fig. 4 PMMA spin-coated glass was illuminated with laser light from one edge, and the scattered light was detected from another edge at different angles, $\theta_1 = 15$ deg and $N = 14.21$ mm, $M = 11.79$ mm. The error in this experiment was 0.8 mm, which is the width of the laser beam.

Table 1 Distance from the incident beam inside of the glass for different incident angle, the error in this calculation is 0.8 cm, given by the width of the laser beam.

Angle of incidence	No. of TIRS	Distance M (cm)
0 deg	0	*n/a*
15 deg	1	14.21
35 deg	2	6.04
45 deg	3	4.77

Values for N for different incident angles from one edge are shown in Table 1. If $N < 26$ mm, the probability that the light is totally internally reflected increases if $90 - \theta_2$ is more than the critical angle.

For incident angles less than 8.3 deg, there is no reflection inside of the collector. For incident angles between 8.3 deg and 24.6 deg, there is one reflection inside of the collector. For the incident angles between 24.6 and 40.5 deg, there are two reflections inside the collector, and for the incident angle of 45 deg, there are three reflections inside the collector.

4 Results

Values of the intensity of scattered light measured over a range of angles are plotted in Fig. 5 for three different angles of incidence of 15, 35, and 45 deg. To compare the results, the maximum intensity for all the measurements was defined as 0 deg. Clearly, the light cone transmitted through the PMMA-coated FSC is considerably broadened compared to a bare glass slide. As seen in Table 2, the angular width of the scattered intensity cone increases for larger angles

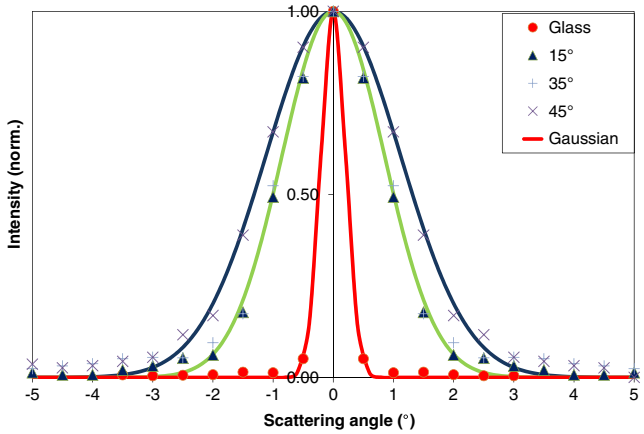

Fig. 5 Angular dependence of normalized intensity for different incident angles for 670 nm of incident light. Lines show Gaussian fits.

Table 2 Beam width for different incident angles of incidence.

Angle of incidence	$1/e$ half-width of the scattered beam (º)
0 deg laser beam	0.6
15 deg	1.3
35 deg	1.4
45 deg	1.6

of incidence up to 45 deg. The width here is determined as the length over which the intensity drops to $1/e$ of the maximum. The measurements at 15 deg and 35 deg show the same width, which can be understood from the fact that the second internal reflection takes place at the opposite glass surface without PMMA. As we will show below, the observed behavior is consistent with diffraction of the laser beam caused by the roughness of the PMMA layer.

In a simple model, we include the diffraction by describing the reflected light as a collection of diffraction-limited cones with an aperture given by the correlation length of the surface roughness (cf. Fig. 6.

Thus, if we consider the PMMA surface as a collection of uncorrelated areas, the angular distribution of the reflected intensity can be fitted to the Fraunhofer diffraction formula for the circular aperture, given by[11]

$$I = I_0 \frac{G^2}{\lambda^2 r^2} \left| \frac{2J_1(ka \sin\theta)}{ka \sin\theta} \right|^2, \tag{6}$$

where $G = \pi a2$, a is the radius of the aperture, r is the distance from observation point to shadow area, λ is the wavelength of the incident, J_1 is the Bessel function of the first order, and k is the optical wavenumber.

Equation (6) gives us the intensity of the scattered light in different detection angles known as the Airy pattern. We note that the use of a Gaussian angular spread in Eq. (1) is a good approximation, as the central lobe of the Airy pattern shows close agreement with a Gaussian profile.[7] Good agreement is obtained for a radius of the aperture of 11 μm for the data taken at a 670-nm wavelength and at a 15-deg angle of incidence, as shown in Fig. 7. Based on our AFM measurements in Fig. 2, we hypothesize that the value of the aperture is related to the characteristic length scale of surface roughness of the PMMA film.

The validity of the diffraction model can be verified by changing the optical wavelength. Figure 8 shows the scattered light intensity measured over a range of angles when we illuminate the sample from one edge at 15 deg through the PMMA part at different wavelengths of 401, 532, 633, and 670 nm, respectively. Clearly, the scattered light cones show a decrease in width as the wavelength decreases.

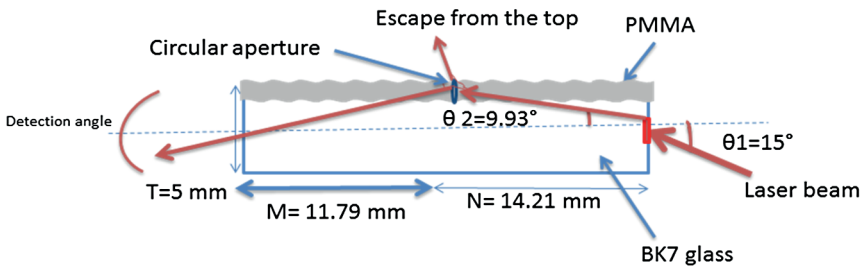

Fig. 6 Scheme showing PMMA spin-coated on top of the glass illuminated with laser light from one edge in incident angle of 15 deg and the forward scattered light detected at different angles. The roughness from spin-coated PMMA is assumed to produce an effective circular aperture when the laser is reflected by the rough layer.

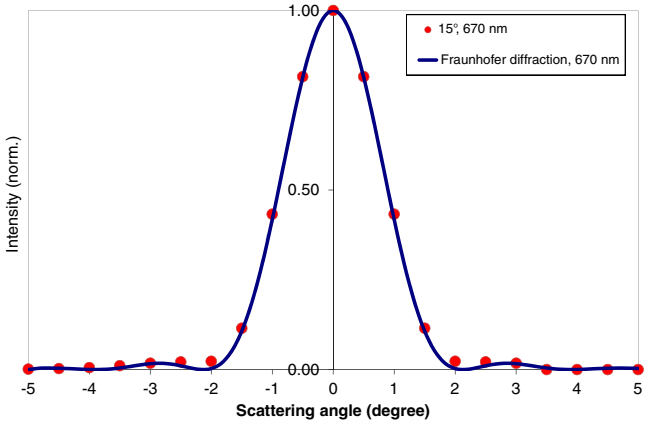

Fig. 7 Normalized angular dependence of *I* in 15-deg incident angles in PMMA side for 670 nm. The solid line was fitted by using Eq. (4). Circles indicate the experimental results.

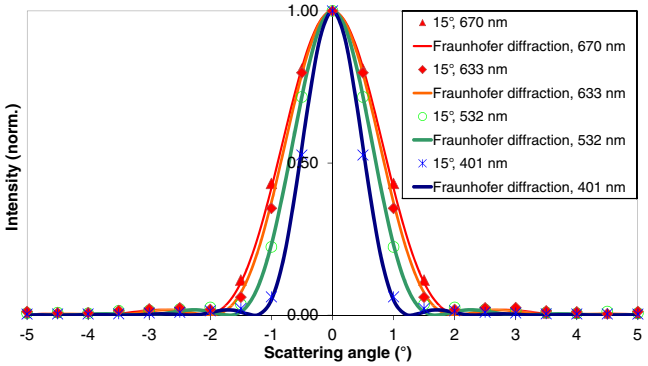

Fig. 8 Comparison of normalized scattering intensity at wavelengths of 670, 633, 532, and 401 nm detected over a range of angles with illumination from 15-deg incident angles through the PMMA part of the sample.

The Fraunhofer diffraction for the circular aperture was calculated when the size of the particle is fixed at 11 μm, while the wavelength was decreased according to the used lasers. We find good quantitative agreement with our experimental results in Fig. 8 (lines), showing that the diffraction pattern gets more and more compressed into a narrow cone around the forward direction for shorter wavelengths.

To further investigate the cause of the scattering in spin-coated PMMA on top of the BK7 glass, the top surface in PMMA ($n = 1.49$) part was covered by optical gel with refractive index of 1.4646 (THORLABS). The surface tension of the gel produced a smooth film that compensated the surface roughness of the PMMA layer. Subsequently, the irradiance of scattered light as a function of angle was measured when illuminating the sample at a 15-deg angle of incidence and at a wavelength of 670 nm. The results are compared with a measurement taken on the same sample before the gel was added. Results are shown in Fig. 9. As we can see, application of the optical gel results in a decrease of the angular width of the scattering cone. This effect unambiguously shows that the cause of the scattering in spin-coated PMMA on top of the glass is the surface roughness. Compared to the surface scattering contribution, the bulk scattering in this type of sample is negligibly small, i.e., of order 10^{-5} cm^{-1}.[10]

It is relevant to consider whether diffraction effects play a role in the situation that the illumination is provided by mutually incoherent fluorescent molecules. To assess this, we have to compare the divergence of a point source with the diffraction provided by the surface roughness. For example, when a point source illuminates an area of 10 μm at a distance of 1 mm from the source, this corresponds to a divergence angle of 10^{-2} radians or 0.5 deg (i.e., smaller than the typical diffraction broadening in our samples). Therefore, surface scattering losses are relevant

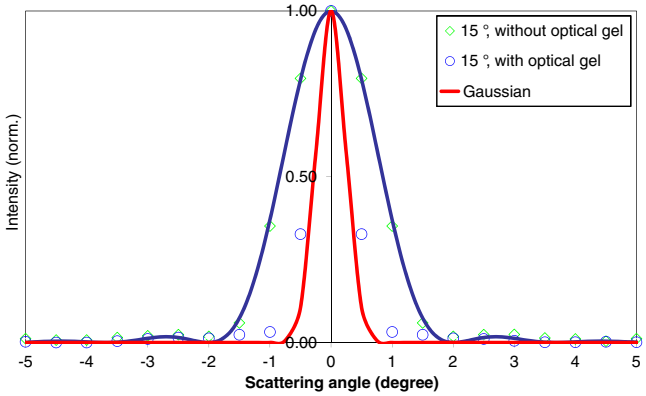

Fig. 9 Comparison of intensity of scattered light at a wavelength of 670 nm detected over a range of angles with illumination from 15-deg incident angles when the PMMA top surface is covered with the optical gel (blue circles) and without optical gel (green diamonds).

for incoherent fluorescence emission at propagation distances larger than several hundred micrometers, which is the case in FSC.

5 Conclusion

The contribution of light scattering in FSCs based on a spin-coated dye/polymer layer was investigated. Measurements of the transmission cones as a function of TIRs revealed that the predominant loss factor is surface scattering at the top layer, caused by the roughness of the spin-coated PMMA. Scattering losses depend on surface roughness, the size of the sample, and the number of TIRs of light inside of the collector. Diffraction of light at surface roughness is shown to increase the escape cone losses, which are one of the most prominent factors limiting FSC performance.[8]

Good agreement is obtained when we consider the PMMA roughness as a coherent aperture with a circular shadow. Therefore, the angular distribution of the scattering intensity can be fitted using far-field Fraunhofer diffraction. The width of the scattered beam increases when the wavelength is increased from 401 to 670 nm, in good agreement with Fraunhofer diffraction for a circular aperture at different wavelengths where the size of the aperture is fixed to the value of 11 μm. This value is of the same order as the correlation length of the height variations observed in AFM measurements. The angular broadening due to surface roughness for a different number of TIRs of light inside of the collector was found to be 0.6 to 1.6 deg (Table 2). The value of the scattering was found to decrease significantly when we covered the top surface with optical gel. This unambiguously shows that surface scattering is the predominant loss factor in our FCS compared to bulk scattering effects. The reduction of angular broadening to 0.6 deg indicates that surface scattering losses could be reduced to below 2% according to our modified Weber and Lambe model. Surface roughness is caused by the large required thickness of the PMMA-dye layer for the operation of the FSC. Our results indicate that the performance of the FSC can be improved by using a subsequent planarization with a thin index-matching layer of low roughness.

Acknowledgments

The authors would like to thank L. Danos for help with the experimental setup. This project was funded partly through UK SUPERGEN (Sustainable Power Generation and Supply) PV21 Programme.

References

1. A. Goetzberger and W. Greubel, "Solar energy conversion with fluorescent collectors," *Appl. Phys.* **14**(2), 123–139 (1977), http://dx.doi.org/10.1007/BF00883080.

2. W. H. Weber and J. Lambe, "Luminescent greenhouse collector for solar radiation," *Appl. Opt.* **15**(10), 2299–2300 (1976), http://dx.doi.org/10.1364/AO.15.002299.
3. J. S. Batchelder, A. H. Zewail, and T. Cole, "Luminescent solar concentrators. 1: theory of operation and techniques for performance evaluation," *Appl. Opt.* **18**(18), 3090–3110 (1979), http://dx.doi.org/10.1364/AO.18.003090.
4. J. S. Batchelder, A. H. Zewail, and T. Cole, "Luminescent solar concentrators. 2: experimental and theoretical analysis of their possible efficiencies," *Appl. Opt.* **20**(21), 3733–3754 (1981), http://dx.doi.org/10.1364/AO.20.003733.
5. P. Kittidachachan et al., "Photon collection efficiency of fluorescent solar collectors," *CHIMIA* **61**(12), 780–786 (2007), http://dx.doi.org/10.2533/chimia.2007.780.
6. W.G. van Sark, K. W. Barnham, and L. H. Slooff, "Luminescent Solar Concentrators–a review of recent results," *Opt. Express* **16**(26), 21773–21792 (2008), http://dx.doi.org/10.1364/OE.16.021773.
7. B. C. Rowan, L. R. Wilson, and B. S. Richards, "Advanced material concepts for luminescent solar concentrators," *IEEE J. Sel. Top. Quantum Electron.* **14**(5), 1312–1322 (2008), http://dx.doi.org/10.1109/JSTQE.2008.920282.
8. J. C. Goldschmidt et al., "Theoretical and experimental analysis of photonic structures for fluorescent concentrators with increased efficiencies," *Phys. Stat. Sol. (a)* **205**(12), 2811–2821 (2008), http://dx.doi.org/10.1002/pssa.v205:12.
9. M. G. Debije et al., "The effect of a scattering layer on the edge output of a luminescent solar concentrator," *Solar Energy Mater. Sol. Cells* **93**(8), 1345–1350 (2009), http://dx.doi.org/10.1016/j.solmat.2009.02.013.
10. Y. Koike, N. Tanio, and Y. Ohtsuka, "Light scattering and heterogeneities in low-loss poly (methyl metacrylate) glasses," *Macromolecules* **22**(3), 1367–1373 (1989), http://dx.doi.org/10.1021/ma00193a060.
11. E. Hecht, Chapter 10 in *Optics*, 4th ed., Addison Wesley, San Francisco (2002).

Nazila Soleimani obtained her PhD degree from the Faculty of Engineering and the Environment in 2012. Since June 2012 she works as a postdoctoral researcher on a NSF sponsored contract at Shasta Crystals, California.

Sebastian Knabe received the diploma in physics from the Carl of Ossietzky University Oldenburg, Germany. He obtained his PhD (Dr.rer. nat.) degree in 2011 with Professor G. H. Bauer on the photoluminescence characterization of excitation states in semiconductors and fluorescence solar collectors.

Gottfried H. Bauer graduated from Stuttgart University on research in the field of plasma physics, thin film semiconductors for optoelectronics and photovoltaics, photochemistry, plasmachemistry. From 1977 onwards he was head of numerous projects and lecturer on graduate level. Since 1993 he is full professor in experimental physics at Carl von Ossietzky University Oldenburg, where he conducts research in the fields of thin film semiconductors, photovoltaics, optoelectronics, polymers and phase decay, nano-scale low dimensional structures.

Tom Markvart is professor of energy conversion in the faculty of engineering and the environment of the University of Southampton. He received his PhD in mathematical physics from the University of Birmingham. He was appointed associate professor at Instituto de Energia Solar at Universidad Politecnica de Madrid in 1991 before returning to Southampton as head of Solar Energy Centre.

Otto L. Muskens is reader in the Department of Physics and Astronomy at the University of Southampton. He received his PhD in experimental physics in 2004 from the University of Utrecht. Since 2009 he leads the Integrated Nanophotonics group in Southampton, with research involving fundamentals and applications of plasmonics and nanophotonics.